Structures of the strange quark stars within a quasiparticle model

Bo-Lin Li,[1,2,*] Zhu-Fang Cui,[3,2,4,†] Zhen-Hua Yu,[3] Yan Yan,[5] Sun An,[1,2,‡] and Hong-Shi Zong[3,2,4,6]

[1]College of Engineering and Applied Sciences, Nanjing University, Nanjing, Jiangsu 210093, China
[2]Nanjing Proton Source Research and Design Center, Nanjing, Jiangsu 210093, China
[3]Department of Physics, Nanjing University, Nanjing, Jiangsu 210093, China
[4]State Key Laboratory of Theoretical Physics, Institute of Theoretical Physics, CAS, Beijing 100190, China
[5]School of Mathematics and Physics, Changzhou University, Changzhou, Jiangsu 213164, China
[6]Joint Center for Particle, Nuclear Physics and Cosmology, Nanjing, Jiangsu 210093, China

(Received 9 December 2018; published 6 February 2019)

The structures of strange quark stars are studied within a quasiparticle model obtained by the two-loop approximation. A softer equation of state yields a smaller maximum mass, a smaller radius, and makes the surface energy density and the surface quark chemical potential larger. The parameter space is obtained under the following constraints: the maximum mass of the strange quark star should be larger than 2.0 solar masses, which matches the masses of PSR J0348 + 0432 and PSR J1614-2230, and the surface energy density should be larger than 2.80×10^{14} g/cm^3. In our parameter space, the surface quark chemical potential is smaller than 308 MeV which is the critical quark chemical potential in QCD without electromagnetism. Also, the tidal Love number k_2 and deformability Λ are calculated for a 1.4-solar-mass strange quark star. A softer equation of state yields a smaller $\Lambda(1.4)$ and leads to a strange quark star that is more compact and less likely to be tidally deformed. The data of GW170817 indicate that the upper bound of $\Lambda(1.4)$ is 800 for the low-spin prior, which gives an upper bound of the parameter ζ of the running coupling constant α_s and gives a lower bound of the vacuum pressure density B, i.e., $\zeta < 0.098$ GeV, $B > (0.111\ \text{GeV})^4$. Moreover, the constraint on ζ also plays an important role in phenomenological studies of the quark-gluon plasma.

DOI: 10.1103/PhysRevD.99.043001

I. INTRODUCTION

Most compact stars are the end points of stellar evolution and are thought to be composed of the densest matter in the cosmos, which provides a natural laboratory for cold and condensed matter studies. Over the past few years, even though considerable efforts have been made to study the structures of the neutronlike stars (the neutron stars and the strange quark stars), their properties are not yet completely understood, due to the lack of a proper equation of state (EOS) in this region. One apparent reason is that quantum chromodynamics (QCD) has complicated nonperturbative effects in the low-energy domain, i.e., the running coupling constant will be significantly enhanced, and experimental data also have large uncertainties there [1]. Therefore, at present, it is still not possible to get a reliable EOS of quark matter from the first principles of QCD. Hence, the commonly used approaches in the study of high-density quark matter are turning to phenomenological models which could incorporate some basic features of QCD. For example, the MIT bag model has been widely used to describe the properties of quark matter. The MIT bag model treats the quarks as free fermions in a bag with negative pressure B, which is called the bag constant, and it also contains the perturbative QCD corrections [2–5]. The Nambu–Jona-Lasinio model possesses chiral symmetry and its breaking, which is the vital feature of low-energy QCD [6–8]. The quasiparticle model with a few fitting parameters has been widely used to simulate the properties of the quark-gluon plasma (QGP) at finite temperature (T) and chemical potential (μ) [9–11]. Besides, it was conjectured that strange quark matter which consists of up (u), down (d) and strange (s) quarks, might be the true ground state of the strong interaction [12,13]. Therefore, the investigation of the EOS for cold and dense strongly interacting quark matter plays a crucial role in the studies of neutronlike stars in astrophysics [14,15].

Recently, the observations of the pulsars PSR J0348 + 0432 ($M = 2.01 \pm 0.04\ M_\odot$) [16] and PSR J1614-2230 ($M = 1.928 \pm 0.017\ M_\odot$) [17] have given a strong constraint on the EOS of strongly interacting matter. From the direct detection of gravitational waves, which originated from a binary system inspiral, by the LIGO and VIRGO network [18], the tidal deformability measurement has also been used to constrain the stiffness of the EOS. Here, in this

*blli@nju.edu.cn
†phycui@nju.edu.cn
‡sunan@nju.edu.cn

paper, we will use the quasiparticle model to describe the EOS of quark matter, and use the above observations to constrain the parameters of the model to obtain a reliable parameter space.

This paper is organized as follows. In Sec. II, we introduce the quasiparticle model and the calculations of the EOS, and the effects of the parameters on the stiffness of the EOS are also been explored. The calculations of M_{TOV}, the tidal Love number and the tidal deformability are exhibited in detail in Sec. III, where various EOS models are extensively investigated with different choices of parameters for the vacuum pressure density B and the nonperturbative effect parameter ζ. Subject to the mass constraints from the observations of pulsars and the tidal deformability $\Lambda(1.4)$ constraints from the astronomical data of GW170817, we derive a reliable parameter space, in which one could choose the desirable parameters for the EOS satisfying specific requirements. Finally, we give a summary of our work in Sec. IV.

II. THE QUASIPARTICLE MODEL

The quasiparticle model which was first proposed by Peshier *et al.* [19] and reformulated by Gorenstein and Yang [20], provides a phenomenological method to study the thermodynamic properties of QGP. Using the quasiparticle model, the authors of Refs. [21,22] have obtained explicit analytic expressions for the EOS at zero T and finite chemical potential by means of the path-integral method with an effective quark propagator. In this paper, we will use this model in which the coupling g is obtained by the two-loop approximation, to construct the EOS to study the structures of the quark stars.

If we have the full quark propagator at finite μ and zero T, the quark number density can be obtained via [21],

$$\rho(\mu) = -N_c N_f \int \frac{\mathrm{d}^4 p}{(2\pi)^4} \mathrm{tr}_D\{\gamma_4 S(p,\mu)\}, \tag{1}$$

where $S(p,\mu)$ is the quark propagator, N_c and N_f represent the numbers of colors and quark flavors respectively, and the trace operator "$\mathrm{tr_D}$" is taken over Dirac indices. Unfortunately, so far the exact form of the quark propagator at finite μ and zero T has not been determined from the first principles of QCD. Hence, an effective quark propagator which has the same form as the free quark propagator in field theory but with a density-dependent effective mass is used as the approximation of the full quark propagator. Here, we choose the effective quark propagator proposed in Ref. [22],

$$S(p,\mu) = \frac{1}{i\gamma\cdot\tilde{p} + m(\mu)}, \tag{2}$$

where $\tilde{p} \equiv (\vec{p}, p_4 + i\mu)$ is the four-momentum of the quark at finite μ, and in Euclidean space, the gamma matrices satisfy $\{\gamma_\mu, \gamma_\nu\} = 2\delta_{\mu\nu}$. Here, we work in the case of the chiral limit, i.e., the masses of the current quarks (u, d, and s) are equal to zero, which would satisfy chemical equilibrium and neutrality naturally. Hence, the effective quark mass which depends on μ reads [9,23,24],

$$m^2(\mu) = \frac{N_f \mu^2 g^2(\mu)}{9\pi^2}, \tag{3}$$

where $g(\mu^2)$ is the effective coupling constant obtained by the two-loop approximation [10,25–27],

$$\alpha_s(\mu) = \frac{g^2(\mu)}{4\pi} = \frac{6\pi}{(33-2N_f)\ln(a\mu)} \times \left[1 - \frac{3(153-19N_f)}{(33-2N_f)^2}\frac{\ln(2\ln(a\mu))}{\ln(a\mu)}\right], \tag{4}$$

where $a = 1.91/(2.91\zeta)$, and ζ is a phenomenological parameter of the quasiparticle model, which characterizes the strength of the nonperturbative effect. The effective coupling constant as a function of quark chemical potential for different ζ is shown in Fig. 1, from which we can see clearly that the effective coupling constant remains substantially smaller than unity in our working region where the quark chemical potential is larger than about 0.3 GeV. This indicates that our theory has a more "fundamental" character.

With this equipment at hand and employing the contour integration method, we can obtain the quark number density

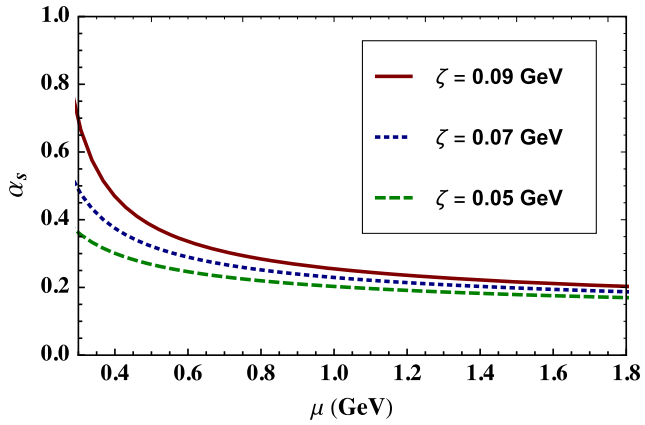

FIG. 1. The effective coupling constant $\alpha_s(\mu)$ as a function of chemical potential is presented. The red-solid line represents the effective coupling constant for $\zeta = 0.09$ GeV, the blue-dotted line represents the effective coupling constant for $\zeta = 0.07$ GeV, while the green-dashed line represents the effective coupling constant for $\zeta = 0.05$ GeV. We can see clearly that the effective coupling constant remains substantially smaller than unity in our working region where the quark chemical potential is larger than about 0.3 GeV.

$$\rho(\mu) = \frac{N_c N_f}{3\pi^2}(\mu^2 - m^2(\mu))^{3/2}\theta(\mu - m(\mu)). \quad (5)$$

Since there is a step function on the right-hand side of Eq. (5), we can see that the quark number density will vanish when μ is smaller than a critical value μ_c. This phenomenon qualitatively agrees with the general conclusion in Ref. [28]. In this model, the critical value depends on the parameter ζ, i.e., $\mu_c \doteq 2.23\zeta$ for $N_c = 3$ and $N_f = 3$. Then, according to Refs. [29,30], we can get the EOS of QCD at finite μ and zero T,

$$P(\mu) = P(\mu)|_{\mu=0} + \int_0^\mu \mathrm{d}\mu' \rho(\mu'), \quad (6)$$

where $P(\mu)|_{\mu=0}$ is the pressure density at $\mu = 0$, which represents the vacuum pressure density. Here we can rewrite it as $P(\mu)|_{\mu=0} \equiv -B(B > 0)$, where B is also a phenomenological parameter in our present work. We should note that B is a positive number, since we treat it as the bag constant in the MIT bag model, while the vacuum pressure must be negative, which preserves the confinement of QCD. It should be noticed that Eq. (6) is a model-independent formula, for the pressure density $P(\mu)$ at finite μ and zero T could be determined by the quark number density $\rho(\mu)$ [up to a constant $P(\mu)|_{\mu=0}$]. Therefore, once the quark number density $\rho(\mu)$ matches the phenomena of QCD, the pressure density surely satisfies the behavior of QCD at finite μ and zero T.

From Eqs. (5) and (6), we can obtain

$$P(\mu) = -B + \frac{N_c N_f}{3\pi^2}\int_0^\mu \mathrm{d}\mu'(\mu'^2 - m^2(\mu'))^{(3/2)}\theta(\mu' - m(\mu')). \quad (7)$$

As we can see from Eq. (7), the EOS constructed from the quasiparticle model depends on the parameter ζ and the so-called vacuum pressure B which also affect the EOS in the study of the quark stars. Then, the energy density of our model is given by

$$\epsilon = -P(\mu) + \mu \cdot \frac{\partial P}{\partial \mu} \quad (8)$$

$$= -P(\mu) + \mu\rho(\mu). \quad (9)$$

Now, let us discuss the effects of the parameters ζ and B on the behavior of the quark number density, the pressure density, the energy density and the EOS of the quark matter. In Fig. 2, we can see clearly that, when $\mu < \mu_c$ ($\mu_c = 2.23\zeta$) the quark number density stays zero, as we discussed below Eq. (5); once $\mu > \mu_c$, the quark number density becomes a monotonically increasing function of μ. The pressure density $P(\mu)$ as a function of μ is presented in Fig. 3. It shows that, when $\mu < \mu_c$, the pressure density equals $-B$, and the pressure density for the smaller ζ grows a little bit faster than the one for the larger ζ. Figure 4 exhibits the behavior of the energy density as a function of μ. Just as in the case of the pressure density, when $\mu < \mu_c$, the energy density equals B. The relation between the pressure and energy density is illustrated in Fig. 5. The red-solid EOS for the smaller ζ becomes stiffer than the blue-dotted one for the larger ζ, and the EOS for the larger B becomes softer than the one for the smaller B. Because the quark number density will vanish when $\mu < \mu_c$, and the vacuum pressure density is negative, i.e., $P(\mu)|_{\mu=0} = -B$, the starting point of the EOS in the pressure–energy density plane is $(P, \epsilon) = (-B, B)$.

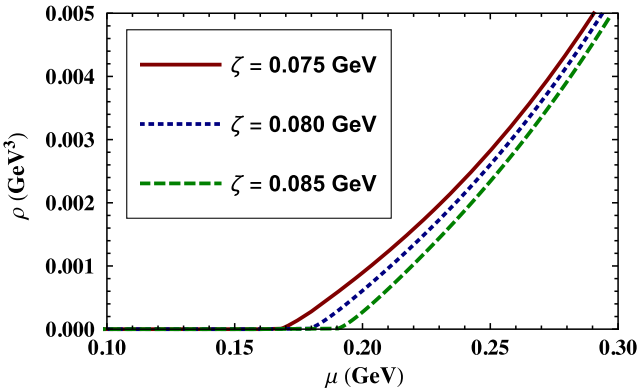

FIG. 2. The quark number density $\rho(\mu)$ as a function of μ is presented. The red-solid line represents the quark number density for $\zeta = 0.075$ GeV, the blue-dotted line represents the quark number density for $\zeta = 0.080$ GeV, while the green-dashed line represents the quark number density for $\zeta = 0.085$ GeV. We can see clearly that the quark number density will stay zero when $\mu < \mu_c$ ($\mu_c = 2.23\zeta$), as we discussed below Eq. (5); once $\mu > \mu_c$, the quark number density becomes a monotonically increasing function of μ.

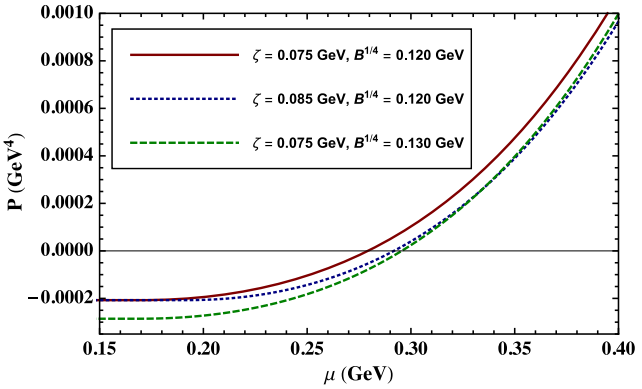

FIG. 3. The pressure density $P(\mu)$ as a function of μ is presented. The red-solid and green-dashed lines represent the pressure density for $\zeta = 0.075$ GeV, but with $B = (0.120\ \mathrm{GeV})^4$ and $B = (0.130\ \mathrm{GeV})^4$, respectively. It shows that, when $\mu < \mu_c$, the pressure density equals $-B$. The blue-dotted line exhibits the pressure density for $\zeta = 0.085$ GeV and $B = (0.120\ \mathrm{GeV})^4$, and compared with the red-solid line, the pressure density for smaller ζ grows a little bit faster than the one for larger ζ.

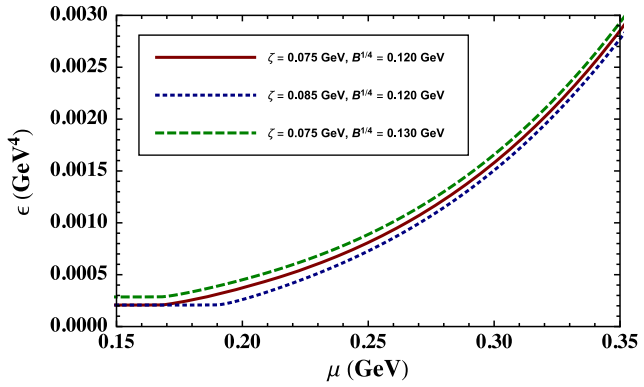

FIG. 4. The energy density $\epsilon(\mu)$ as a function of μ is exhibited. Just as in the case of the pressure density, the red-solid and green-dashed lines represent the energy density for $\zeta = 0.075$ GeV, but with $B = (0.120\ \text{GeV})^4$ and $B = (0.130\ \text{GeV})^4$, respectively. It shows that, when $\mu < \mu_c$, the energy density equals B. The blue-dotted line exhibits the energy density for $\zeta = 0.085$ GeV and $B = (0.120\ \text{GeV})^4$.

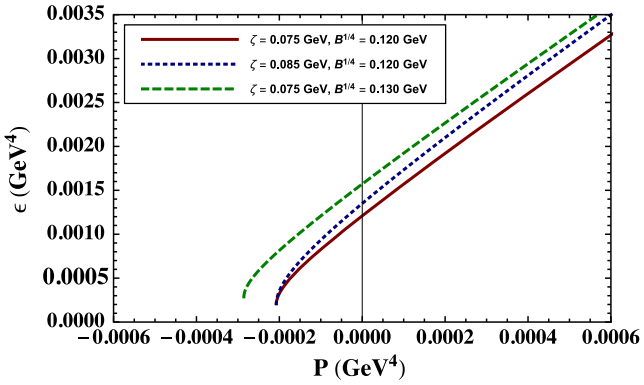

FIG. 5. The energy density ϵ as a function of pressure density P is shown. The red-solid and blue-dotted lines represent the EOS for $B = (0.120\ \text{GeV})^4$, but with $\zeta = 0.075$ GeV and $\zeta = 0.085$ GeV, respectively. The red-solid EOS for smaller ζ becomes stiffer than the blue-dotted one for larger ζ. The green-dashed line exhibits the EOS for $\zeta = 0.075$ GeV and $B = (0.130\ \text{GeV})^4$; compared with the red-solid line, the EOS for larger B becomes softer than the one for smaller B. Because the quark number density will vanish when $\mu < \mu_c$, and the vacuum pressure is negative, i.e., $P(\mu)|_{\mu=0} = -B$, the staring point of the EOS in the pressure-energy density plane is $(P, \epsilon) = (-B, B)$.

III. THE STRUCTURES OF STRANGE QUARK STARS

During the inspiral and merger of two stars, the EOS-dependent tidal deformability Λ describes the ratio of each star's induced mass quadrupole moment to the tidal field of its companion [31–35]. When a low-spin prior is considered for both stars in the binary inspiral, and it is reasonable to think about the magnetic breaking during the merger evolution, the tidal deformability Λ for a 1.4 $M_\odot$ star [denoted as $\Lambda(1.4)$ below] is restricted to be smaller than 800, while in the high-spin prior case, it is determined to be smaller than 1400 [18]. The tidal deformability Λ related to the $l = 2$ dimensionless tidal Love number k_2, is given by (in units $G = c = 1$),

$$k_2 = \frac{3}{2}\Lambda\left(\frac{M}{R}\right)^5. \tag{10}$$

The Love number describes how easily the substantial part of a star is deformed by an external tidal field. As discussed in Refs. [33,34,36], with our EOS table, we could obtain the structure of a quark star by integrating the Tolman-Oppenheimer-Volkoff equation

$$\frac{\mathrm{d}P(r)}{\mathrm{d}r} = -\frac{(\epsilon + P)(M + 4\pi r^3 P)}{r(r - 2M)}, \tag{11}$$

$$\frac{\mathrm{d}M(r)}{\mathrm{d}r} = 4\pi r^2 \epsilon, \tag{12}$$

and

$$\frac{\mathrm{d}H(r)}{\mathrm{d}r} = \beta, \tag{13}$$

$$\begin{aligned}\frac{\mathrm{d}\beta(r)}{\mathrm{d}r} = {} & 2\left(1 - 2\frac{M}{r}\right)^{-1} H\left\{-2\pi[5\epsilon + 9P + f(\epsilon + P)]\right. \\ & \left. + \frac{3}{r^2} + 2\left(1 - 2\frac{M}{r}\right)^{-1}\left(\frac{M}{r^2} + 4\pi r P\right)^2\right\} \\ & + \frac{2\beta}{r}\left(1 - 2\frac{M}{r}\right)^{-1}\left\{-1 + \frac{M}{r} + 2\pi r^2(\epsilon - P)\right\},\end{aligned} \tag{14}$$

where f is given by

$$f = \frac{\mathrm{d}\epsilon}{\mathrm{d}P} \tag{15}$$

for slow changes in matter configurations. The augmented Eqs. (13) and (14) are integrated outward starting just outside the center via the expansions $H(r) = a_0 r^2$, and $\beta(r) = 2a_0 r$ as $r \to 0$, where a_0 is a constant which determines how much the star is deformed by an external tidal field and can be chosen arbitrarily as it cancels in the expression for the Love number k_2. Hence, in our calculations, we choose $a_0 = 1$ for simplicity.

For the internal solution, the $l = 2$ tidal Love number k_2 is,

$$\begin{aligned}k_2 = {} & \frac{8C^5}{5}(1 - 2C)^2[2 + 2C(y - 1) - y] \\ & \times \{2C[6 - 3y + 3C(5y - 8)] \\ & + 4C^3[13 - 11y + C(3y - 2) + 2C^2(1 + y)] \\ & + 3(1 - 2C)^2[2 - y + 2C(y - 1)]\ln(1 - 2C)\}^{-1},\end{aligned} \tag{16}$$

where $C = M/R$ is the compactness of the star, and

$$y = \frac{R\beta(R)}{H(R)} - \frac{4\pi R^3 \epsilon_0}{M}, \tag{17}$$

for in the case of the strange quark stars, there is a nonzero energy density ϵ_0 just inside the surface.

The mass-radius relation is shown in Fig. 6. It is obviously that a larger B yields a smaller maximum mass and radius, and a larger ζ yields a smaller maximum mass and radius. Figure 7 exhibits the surface energy density ϵ_0 as a function of B. And we can see that a larger B makes the surface energy density larger, and a larger ζ makes the surface energy density larger. This behavior could be understood from Fig. 5. In Fig. 5, we can see that the EOS becomes softer for a larger ζ or a larger B, which means that just inside the surface of the strange quark star where the pressure is nearly zero, the surface energy density ϵ_0 becomes larger for a larger ζ or a larger B. This phenomenon will help us to derive constraints on the parameters ζ and B. Hence, we can obtain our parameter space (see the orange region in Fig. 11) under the following constraints: the obtained maximum mass (denoted as M_{TOV}) should be larger than 2.0 solar masses, which matches the masses of PSR J0348 + 0432 ($M = 2.01 \pm 0.04\ M_\odot$) [16], and PSR J1614-2230 ($M = 1.928 \pm 0.017\ M_\odot$) [17]; and the surface energy density should be larger than 2.80×10^{14} g/cm^3.

We have calculated some strange quark stars for different ζ and B, and some results are shown in Table I. The masses of these strange quark stars are larger than 2.0 solar masses, and the radii are near 12 km. Because the pressure density at the surface of a strange quark star is nearly zero, the surface quark chemical potential can be simply given by,

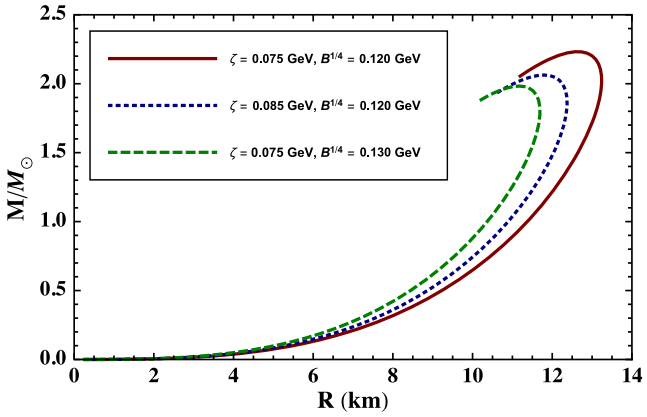

FIG. 6. The mass-radius relation of the strange quark star is presented. The red-solid and green-dashed lines represent the mass-radius relation for $\zeta = 0.075$ GeV, but with $B = (0.120\ \mathrm{GeV})^4$ and $B = (0.130\ \mathrm{GeV})^4$, respectively. The blue-dotted line exhibits the mass-radius relation with $\zeta = 0.085$ GeV and $B = (0.120\ \mathrm{GeV})^4$. It is obvious that both larger ζ and larger B make the mass and radius of the quark star smaller.

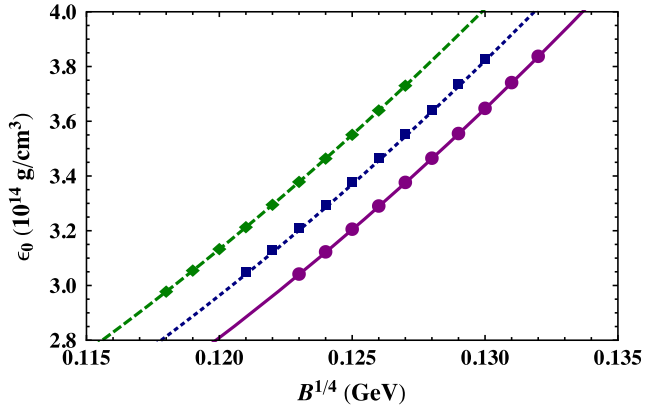

FIG. 7. The surface energy density of the strange quark star is presented as a function of B. The purple-solid line represents the surface energy density for $\zeta = 0.075$ GeV, the blue-dotted line exhibits the surface energy density for $\zeta = 0.080$ GeV, and the green-dashed line shows the surface energy density for $\zeta = 0.085$ GeV. We can see that both larger ζ and larger B make the surface energy density larger.

$$\mu_0 \doteq \frac{\epsilon_0}{\rho_0}, \tag{18}$$

where ϵ_0 is the surface energy density, and ρ_0 is the quark number density at the surface of the strange quark star. The surface quark chemical potential for a larger ζ or a larger B will become larger, which is the same behavior as for the surface energy. In Table I, all the surface quark chemical potentials are smaller than 308 MeV, which is the critical one in QCD without electromagnetism [28]. The same holds for the other surface quark chemical potentials for the parameters ζ and B in the orange region of Fig. 11.

In order to make a comparison between our strange quark matter EOS and the ordinary nuclear matter, we take the data from the EOS described using the compressible liquid-drop model (CLDM) of nuclei with the parameters calculated using the SLy effective nucleon-nucleon interactions [37], and extract the relation between the energy per baryon and baryon number density from the red-solid line in Fig. 8. This relation extracted from our strange quark matter EOS is also presented. The set of parameters we choose are typical. We can see from our parameter space,

TABLE I. Properties of the strange quark stars, including the radius R, the maximum mass M_{TOV}, the surface energy density ϵ_0 and the surface quark chemical potential μ_0, for different choices of ζ and B.

$B^{1/4}$ (GeV)	ζ (GeV)	R (km)	M_{TOV} ($M_\odot$)	ϵ_0 (10^{14}g/cm^3)	μ_0 (GeV)
0.122	0.082	11.829	2.0666	3.1882	0.29096
0.122	0.080	11.966	2.0993	3.1203	0.28847
0.122	0.078	12.102	2.1316	3.0548	0.28604
0.124	0.078	11.863	2.0821	3.2176	0.28921
0.126	0.078	11.497	2.0353	3.3875	0.29240

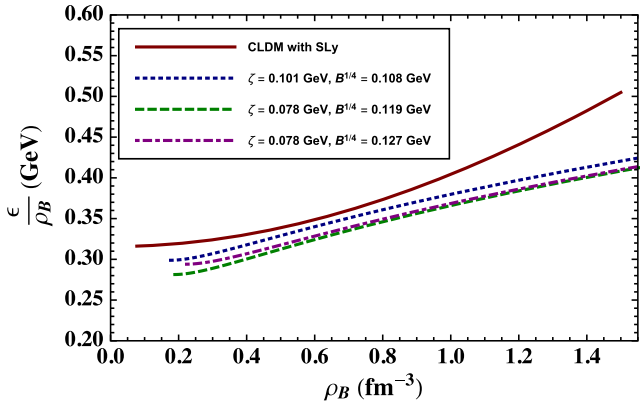

FIG. 8. The relation between the energy per baryon and baryon number density is exhibited. The red-solid line shows the relation extracted from an EOS described using the CLDM of nuclei with the parameters calculated using the SLy effective nucleon-nucleon interactions. The blue-dotted, green-dashed, and purple-dot-dashed lines represent the relations extracted from our strange quark EOS for $(\zeta, B^{1/4}) = (0.101, 0.108), (0.078, 0.119)$, and $(0.078, 0.127)$, respectively. It is obvious that the absolute minimum in energy per baryon for our strange quark matter EOS is smaller than that for the EOS of ordinary nuclear matter described by the CLDM, and the EOS for smaller ζ and smaller B has a lower absolute minimum in energy.

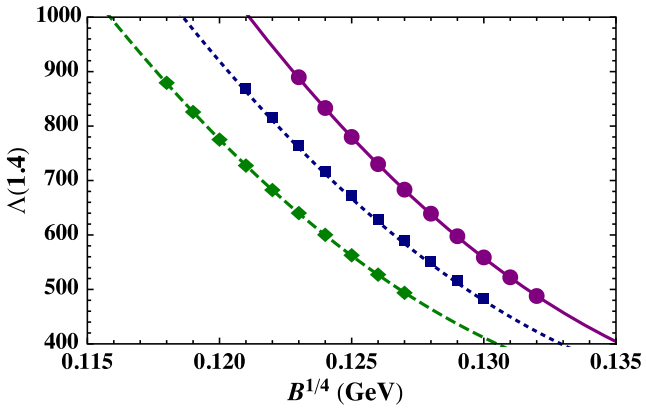

FIG. 9. The tidal deformability for a 1.4-solar-mass strange quark star $\Lambda(1.4)$ as a function of B is illustrated. The purple-solid line represents $\Lambda(1.4)$ for $\zeta = 0.075$ GeV, the blue-dotted line exhibits $\Lambda(1.4)$ for $\zeta = 0.080$ GeV, and the green-dashed line shows $\Lambda(1.4)$ for $\zeta = 0.85$ GeV. It shows that $\Lambda(1.4)$ decrease with increasing B.

i.e., Fig. 11 that $(\zeta, B^{1/4}) = (0.101, 0.108)$ is the intersection point of the red-solid line and the blue-dotted line, $(\zeta, B^{1/4}) = (0.078, 0.119)$ is the intersection point of the red-solid line and the purple-dot-dashed line, and $(\zeta, B^{1/4}) = (0.078, 0.127)$ stays on the blue-dotted line. And it is obvious that the absolute minimum of the energy per baryon for our strange quark matter EOS is smaller than that for the EOS of ordinary nuclear matter described by the CLDM, which fulfills the Bodmer-Witten hypothesis [12,13]. Also, the EOS for smaller ζ and smaller B has a lower absolute minimum in energy.

The properties of a 1.4-solar-mass strange quark star are listed in Table II. It shows that the softer EOS will make a strange quark star more compact for a given mass and less likely to be tidally deformed, which can be seen clearly from Figs. 9 and 10. Figures 9 and 10 illustrate that the tidal deformability for a 1.4-solar-mass strange quark star decreases with both increasing ζ and increasing B [38,39].

TABLE II. Properties of a 1.4 $M_\odot$ strange quark star, including the compactness M/R, the Love number k_2 and the tidal deformability Λ, for different choices of ζ and B.

$B^{1/4}$ (GeV)	ζ (GeV)	M/R	k_2	Λ
0.122	0.082	0.17502	0.18669	757.76
0.122	0.080	0.17337	0.19041	810.35
0.122	0.078	0.17178	0.19403	864.93
0.124	0.078	0.17513	0.18761	759.08
0.126	0.078	0.17855	0.18119	665.66

Figure 11 illustrates the parameter space of our quasiparticle model. The parameters ζ and B below the red-solid line yield a maximum mass larger than 2.0 solar masses, while the parameters above the red-solid line yield a maximum mass smaller than 2.0 solar masses. The surface energy ϵ_0 is larger than 2.80×10^{14} g/cm^3 for the parameters above the blue-dotted line, while the surface energy ϵ_0 is smaller than 2.80×10^{14} g/cm^3 for the parameters below the blue-dotted line. The tidal deformability for a 1.4 solar mass strange quark star is larger than 800 and 600 for the parameters above the green-dashed line and the purple-dot-dashed line, respectively, and the tidal deformability for a 1.4 solar mass strange quark star is smaller than 800 and 600 for the parameters below the green-dashed line and the purple-dot-dashed line, respectively. The intersection

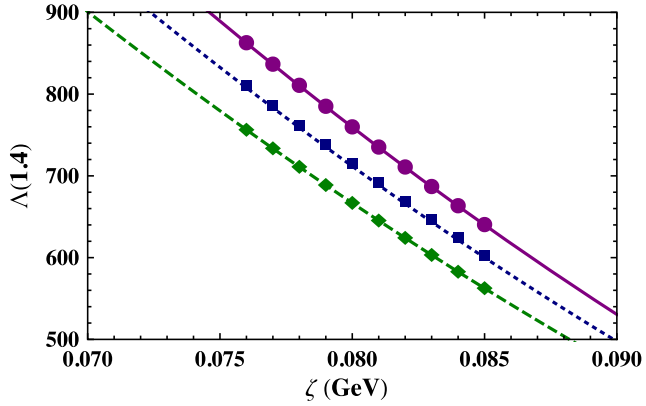

FIG. 10. The tidal deformability for a 1.4-solar-mass strange quark star $\Lambda(1.4)$ as a function of ζ is shown. The purple-solid line represents $\Lambda(1.4)$ for $B = (0.123\ \text{GeV})^4$, the blue-dotted line exhibits $\Lambda(1.4)$ for $B = (0.124\ \text{GeV})^4$, and the green-dashed line shows $\Lambda(1.4)$ for $B = (0.125\ \text{GeV})^4$. It exhibits that $\Lambda(1.4)$ decreases with increasing ζ.

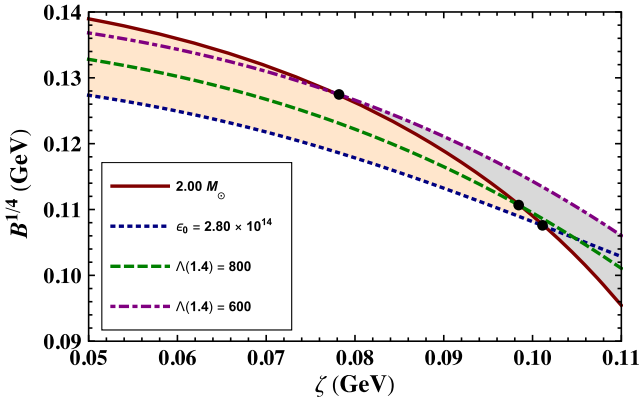

FIG. 11. The parameter space of our quasiparticle model is presented. The parameters ζ and B below the red-solid line yield a maximum mass larger than 2.0 solar masses, while the parameters above the red-solid line yield a maximum mass smaller than 2.0 solar masses. The surface energy ϵ_0 is larger than 2.80×10^{14} g/cm^3 for the parameters under the blue-dotted line, while the surface energy ϵ_0 is smaller than 2.80×10^{14} g/cm^3 for the parameters below the blue-dotted line. The tidal deformability for a 1.4 solar mass strange quark star [$\Lambda(1.4)$] is larger than 800 and 600 for the parameters under the green-dashed line and the purple-dot-dashed line, respectively, and the tidal deformability for a 1.4 solar mass strange quark star [$\Lambda(1.4)$] is smaller than 800 and 600 for the parameters below the green-dashed line and the purple-dot-dashed line, respectively. The intersection points of the red-solid line and the blue-dotted line, green-dashed line, and purple-dot-dashed line are about $(\zeta, B^{1/4}) = (0.101, 0.108)$, (0.098, 0.111), (0.078, 0.127), respectively.

points of the red-solid line and the blue-dotted line, green-dashed line, and purple-dot-dashed line are about $(\zeta, B^{1/4}) = (0.101, 0.108)$, (0.098, 0.111), (0.078, 0.127), respectively. These three intersections could give a constraint on ζ of the running coupling constant α_s and on the vacuum pressure density B via the observations about strange quark stars. If a strange quark star exists, then, the parameter ζ should be smaller than 0.101 GeV and the vacuum pressure density B should be larger than $(0.108\ \text{GeV})^4$. The data of GW170817 [18] indicates that the upper bound of the tidal deformability $\Lambda(1.4)$ is 800, and thus ζ must be smaller than 0.098 GeV and B must be larger than $(0.111\ \text{GeV})^4$. And if the tidal deformability $\Lambda(1.4)$ is smaller than 600, then ζ should be smaller than 0.078 GeV and B should be larger than $(0.127\ \text{GeV})^4$. The constraint on ζ also plays an important role in phenomenological studies of QGP.

IV. SUMMARY

In this work, we have studied the structures of the strange quark stars using the quasiparticle model. In our model, the EOS will become softer for a larger ζ or a larger B, which leads to the result that a larger ζ or a larger B yields a smaller maximum mass and a smaller radius. We can see that it is easy to obtain an EOS for a strange quark star whose mass is larger than 2.0 solar masses. And a larger ζ or a larger B will make the surface energy density and the surface quark chemical potential larger. In our parameter space, i.e., for the parameters in the orange region of Fig. 11, the surface quark chemical potential is smaller than 308 MeV, which is the critical quark chemical potential in QCD without electromagnetism [28]. Also, the tidal Love number k_2 and deformability Λ were calculated for a 1.4-solar-mass strange quark star. The tidal deformability $\Lambda(1.4)$ decreases with increasing ζ and increasing B, which indicates that the softer EOS will lead to a strange quark star that is more compact and less likely to be tidally deformed. At last, we have scanned the parameter space, i.e., the $(\zeta, B^{1/4})$ plane, looking for the suitable parameters ζ and B which yield the strange quark stars that satisfy the constraints from the observable data. In the orange region of Fig. 11, for the parameters in the domain between the red-solid line and green-dashed line, the mass of the strange quark star is larger than 2.0 solar masses, which matches the masses of PSR J0348 + 0432 ($M = 2.01 \pm 0.04\ M_\odot$) [16] and PSR J1614-2230 ($M = 1.928 \pm 0.017\ M_\odot$) [17], the tidal deformability $\Lambda(1.4)$ is smaller than 800, which satisfies the constraint from the data of GW170817 [18], and the intersection of the red-solid line and the green-dashed line gives an upper bound of ζ of the coupling constant α_s and gives a lower bound of the vacuum pressure density B, i.e., $\zeta < 0.098$ GeV, $B > (0.111\ \text{GeV})^4$; for the parameters in the domain between the red-solid line and the purple-dot-dashed line, the tidal deformability $\Lambda(1.4)$ is smaller than 600. If further gravitational-wave data constrain $\Lambda(1.4) < 600$, the intersection of the red-solid line and the purple-dot-dashed line could also give an upper bound of ζ of the coupling constant α_s and give a lower bound of the vacuum pressure density B, i.e., $\zeta < 0.078$ GeV, $B > (0.127\ \text{GeV})^4$. Furthermore, the constraint on ζ also plays an important role in phenomenological studies of quark-gluon plasma.

ACKNOWLEDGMENTS

This work is supported by the National Natural Science Foundation of China (under Grants No. 11805097, No. 11475085, and No. 11535005), the China Postdoctoral Science Foundation (under Grant No. 2018M642204), and the Jiangsu Provincial Natural Science Foundation of China (under Grant No. BK20180323).

[1] S. Bethke, Prog. Part. Nucl. Phys. **58**, 351 (2007).
[2] A. Chodos, R. L. Jaffe, K. Johnson, C. B. Thorn, and V. F. Weisskopf, Phys. Rev. D **9**, 3471 (1974).
[3] M. Alford, M. Braby, M. Paris, and S. Reddy, Astrophys. J. **629**, 969 (2005).
[4] C. Alcock, E. Farhi, and A. Olinto, Astrophys. J. **310**, 261 (1986).
[5] E.-P. Zhou, X. Zhou, and A. Li, Phys. Rev. D **97**, 083015 (2018).
[6] S. B. Rüster and D. H. Rischke, Phys. Rev. D **69**, 045011 (2004).
[7] M. Hanauske, L. M. Satarov, I. N. Mishustin, H. Stöcker, and W. Greiner, Phys. Rev. D **64**, 043005 (2001).
[8] D. P. Menezes, C. Providncia, and D. B. Melrose, J. Phys. G **32**, 1081 (2006).
[9] A. Peshier, B. Kämpfer, and G. Soff, Phys. Rev. C **61**, 045203 (2000).
[10] H.-H. Ma and W.-L. Qian, Braz. J. Phys. **48**, 160 (2018).
[11] Y. Yan, J. Cao, X.-L. Luo, W.-M. Sun, and H. Zong, Phys. Rev. D **86**, 114028 (2012).
[12] A. R. Bodmer, Phys. Rev. D **4**, 1601 (1971).
[13] E. Witten, Phys. Rev. D **30**, 272 (1984).
[14] F. Özel, Nature (London) **441**, 1115 (2006).
[15] M. Alford, D. Blaschke, A. Drago, T. Klähn, G. Pagliara, and J. Schaffner-Bielich, Nature (London) **445**, E7 (2007).
[16] J. Antoniadis *et al.*, Science **340**, 1233232 (2013).
[17] E. Fonseca, T. T. Pennucci, J. A. Ellis, I. H. Stairs, D. J. Nice, S. M. nsom, P. B. Demorest, Z. Arzoumanian, K. Crowter, T. Dolch, R. D. Ferdman, M. Gonzalez, G. Jones, M. L. Jones, M. T. Lam, L. Levin, M. A. McLaughlin, K. ovall, J. K. Swiggum, and W. Zhu, Astrophys. J. **832**, 167 (2016).
[18] B. P. Abbott, R. Abbott, T. D. Abbott, F. Acernese, K. Ackley, C. Adams, T. Adams, P. Addesso *et al.* (LIGO Scientific Collaboration and Virgo Collaborations), Phys. Rev. Lett. **119**, 161101 (2017).
[19] A. Peshier, B. Kampfer, O. Pavlenko, and G. Soff, Phys. Lett. B **337**, 235 (1994).
[20] M. I. Gorenstein and S. N. Yang, Phys. Rev. D **52**, 5206 (1995).
[21] H.-S. Zong and W.-M. Sun, Int. J. Mod. Phys. A **23**, 3591 (2008).
[22] A.-M. Zhao, J. Cao, L.-J. Luo, W.-M. Sun, and H.-S. Zong, Mod. Phys. Lett. A **25**, 47 (2010).
[23] P. Lévai and U. Heinz, Phys. Rev. C **57**, 1879 (1998).
[24] V. M. Bannur, Phys. Rev. C **78**, 045206 (2008).
[25] V. M. Bannur, Phys. Rev. C **75**, 044905 (2007).
[26] W. E. Caswell, Phys. Rev. Lett. **33**, 244 (1974).
[27] R. A. Schneider, arXiv:hep-ph/0303104.
[28] M. A. Halasz, A. D. Jackson, R. E. Shrock, M. A. Stephanov, and J. J. M. Verbaarschot, Phys. Rev. D **58**, 096007 (1998).
[29] M. He, W. min Sun, H. tao Feng, and H. shi Zong, J. Phys. G **34**, 2655 (2007).
[30] H.-s. Zong and W.-m. Sun, Phys. Rev. D **78**, 054001 (2008).
[31] T. Damour, M. Soffel, and C. Xu, Phys. Rev. D **45**, 1017 (1992).
[32] E. E. Flanagan and T. Hinderer, Phys. Rev. D **77**, 021502 (2008).
[33] T. Hinderer, Astrophys. J. **677**, 1216 (2008).
[34] T. Damour and A. Nagar, Phys. Rev. D **80**, 084035 (2009).
[35] T. Binnington and E. Poisson, Phys. Rev. D **80**, 084018 (2009).
[36] K. Yagi and N. Yunes, Science **341**, 365 (2013).
[37] F. Douchin and P. Haensel, Astron. Astrophys. **380**, 151 (2001).
[38] T. Hinderer, B. D. Lackey, R. N. Lang, and J. S. Read, Phys. Rev. D **81**, 123016 (2010).
[39] S. Postnikov, M. Prakash, and J. M. Lattimer, Phys. Rev. D **82**, 024016 (2010).